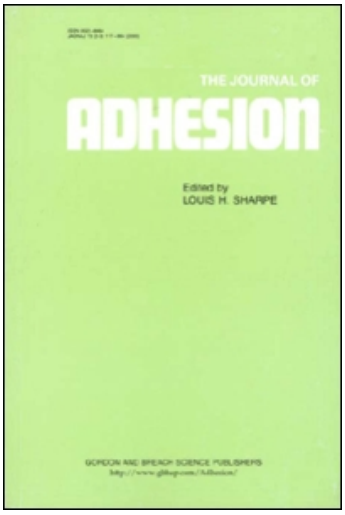

The Journal of Adhesion
Publication details, including instructions for authors and subscription information:
http://www.informaworld.com/smpp/title~content=t713453635

Evaluation of Mode-II Fracture Energy of Adhesive Joints with Different Bond Thickness

Hamid Reza Daghyani[a]; Lin Ye[a]; Yiu-Wing Mai[a]
[a] Centre for Advanced Materials Technology, Department of Mechanical and Mechatronic Engineering, The University of Sydney, Australia

To cite this Article Daghyani, Hamid Reza , Ye, Lin and Mai, Yiu-Wing(1996) 'Evaluation of Mode-II Fracture Energy of Adhesive Joints with Different Bond Thickness', The Journal of Adhesion, 56: 1, 171 — 186
To link to this Article: DOI: 10.1080/00218469608010506
URL: http://dx.doi.org/10.1080/00218469608010506

J. Adhesion, 1996, Vol. 56, pp. 171–186
Reprints available directly from the publisher
Photocopying permitted by license only

Evaluation of Mode-II Fracture Energy of Adhesive Joints with Different Bond Thickness

HAMID REZA DAGHYANI, LIN YE* and YIU-WING MAI

Centre for Advanced Materials Technology, Department of Mechanical and Mechatronic Engineering, The University of Sydney, NSW 2006, Australia

(Received October 3, 1994; in final form October 30, 1995)

A study on the mode-II edge-sliding fracture behaviour of aluminium-adhesive joints was carried out. Compact pure shear (CPS) adhesive joints of different bond thickness were produced using a rubber-modified epoxy resin as the adhesive. An analytical model was developed to calculate the stress distribution along the bond line of the joint. A crack-closure technique was used to evaluate the mode-II strain energy release rate, G_{II}, as a function of the adhesive bond thickness. The results indicated that for a given applied load, G_{II} increased gradually with the bond thickness. A finite element model (FEM) was also developed to evaluate the stress state along the bond line and the strain energy release rate of the CPS specimens. Consistent results were obtained between the theoretical model and finite element analysis. Scanning electron micrographs of the fracture surface illustrated a mainly interfacial fracture path between the adherends and the adhesive for all adhesive joint specimens. The critical fracture load increased very rapidly with bond thickness in the range 0.02 mm to 0.1 mm but remained constant thereafter. However, the mode-II critical fracture energy rose more gradually as the bond thickness was increased.

KEY WORDS: Adhesive joints; mode-II fracture toughness; bond thickness; strain energy release rate; rubber-modified epoxy.

1. INTRODUCTION

Application of adhesive joints has been well developed for many engineering structural components in aircraft, automobiles and modern space industries in the last few decades. The analysis of adhesive joints is complicated, because the design process and applications involve many geometric, material and fabrication variables. The strength of adhesive joints is traditionally characterised by an appropriate yield criterion using shear-lap, peel and tensile tests,[1] but it is unfortunately strongly dependent on specimen geometry. Furthermore, when the adhesive material is confined within a thin bond line, brittle fracture occurs. Therefore, a criterion based on fracture energy rather than strength is more suitable for describing adhesive failure.

The critical strain energy release rate is normally used to characterise the crack propagation resistance of adhesives[2–7] and the critical stress intensity factors were also applied to evaluate the fracture toughness of aluminium-adhesive joints.[8–10] In practice, adhesive failure is generally associated with mode-I and/or mode-II fractures

* Corresponding author.

along the debonded interface or cohesively within the adhesive layer. Hence, several test specimen geometries such as the double-cantilever-beam (DCB),[1-7] compact tension (CT),[11-13] compact shear (CS),[9] cracked lap shear (CLS)[14] and end-notched flexural (ENF)[15,16] have been designed to determine the fracture resistance of adhesive joints.

Mode-I fracture has been studied in many previous papers,[1-13,17,18] but little work has been reported to date on the pure sliding mode-II fracture, which is of more significance in many engineering applications. Although some efforts have been made to study mode-II fracture of adhesive joints,[8-11,14,17-22] the fracture of the specimens obtained in these studies was actually a mixed-mode rather than a pure sliding mode. However, some investigators used either the CS[9,11] or ENF geometry[15,16] and were able to produce a predominant mode-II fracture. Ripling *et al.*[23] proposed a compact pure shear specimen (CPS) to evaluate the mode-II critical fracture energy, G_{IIC}, of an adhesive joint which is given by:

$$G_{IIC} = \frac{P_{IIC}^2}{b^2 H E_{al}} \tag{1}$$

where P_{IIC} is the fracture load, E_{al} the Young's modulus, b the thickness and H the height of the adherends. Equation (1) was obtained from the compliance method with a uniform stress distribution along the height of the adherends (H), which may give a lower estimation of G_{IIC}. Also, no account is taken of the effect of the thickness of the adhesive, t. Obviously, further work is required to understand comprehensively the fracture mechanisms of pure shear fracture in adhesive joints. Even though finite element models have broadly been developed to evaluate the fracture energy of joints,[4,11-13,24-27] an analytical approach is often preferred for design purposes.

In the present work, the mode-II fracture behaviour of aluminium-epoxy adhesive joints with different bond thickness is investigated using the compact pure shear (CPS) specimen geometry. An analytical model is developed to obtain the stress distribution along the adhesive bond line. The mode-II critical strain energy release rate, G_{IIC}, is determined assuming an interface crack, and the effect of the bond thickness on G_{IIC} is evaluated. Scanning electron microscopy (SEM) is used to assess the effect of mode-II sliding on the fracture morphology of the joints.

2. EXPERIMENTAL PROCEDURE

Figure 1 shows a compact pure shear (CPS) specimen which produces a pure sliding fracture. A similar specimen was developed by Ripling *et al.*[23] to study mixed mode (modes-I and II) fractures. The base adhesive material used for the CPS adhesive joints was a diglycidyl ether of bisphenol A (DGEBA) epoxy resin (Araldite® GY260, Ciba-Geigy, Australia) modified with a rubber system (CTBN, 1300 X 13, BF. Goodrich). The property profile of the adhesive material has been reported in a previous study[28] and preparation of the CPS adhesive joint specimens was similar to that of the CT specimens used in our previous work[12] for mode-I fracture, which provides strong interfacial bonding between the adhesive and the adherends and results in a cohesive fracture path for CT joints under mode-I loading. Some typical properties of the adhesive and the adherend are listed in Table I. It is noted that this epoxy resin

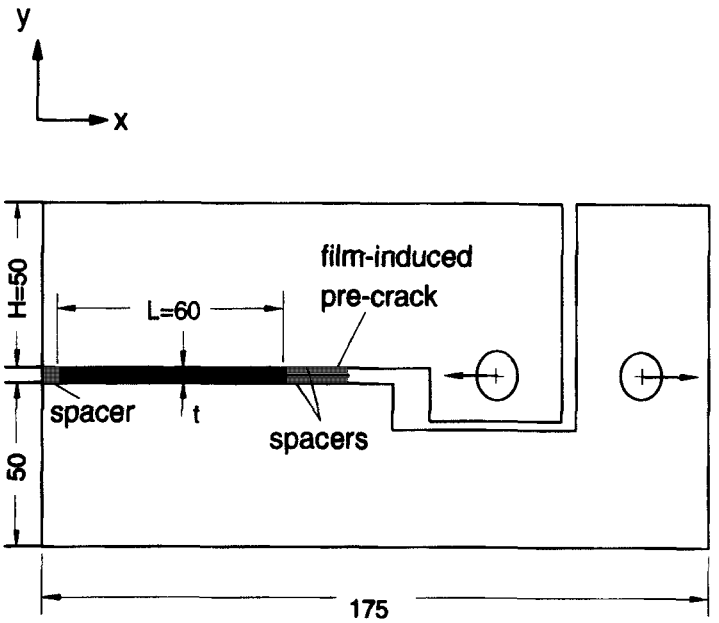

FIGURE 1 Schematic illustration of a CPS specimen. ($b = 10$ mm).

TABLE I
Mechanical properties of adhesive and adherend

Material	E(GPa)	σ_u(MPa)	ν
GY260 + 2% Rubber	3.15	81	0.35
Aluminium Alloy 5083	71.7	275	0.3

E: Young's modulus
σ_u: Ultimate tensile strength
ν: Poisson's ratio

(GY260) has a very high mode-I fracture toughness ($G_{IC} = 1.76\,kJ/m^2$) compared with other epoxy systems, *e.g.* GY250 ($G_{IC} = 0.23\,kJ/m^2$)[29] and Epon 828 ($G_{IC} = 0.2\,kJ/m^2$).[30] The mode-I toughness for the rubber toughened (2%) GY260 has a value of $2.76\,kJ/m^2$.[12,28] A thin Teflon film, 20 μm in thickness and coated with release agent, was used to generate a film-induced pre-crack in the specimens as shown in Figure 1. The fracture loads of the CPS adhesive joints were measured using a 1195 Instron machine at 22°C ± 2° with a crosshead speed of 2 mm/min. The fracture surfaces of the specimens were coated with a thin layer of platinum to increase surface conductivity. A JEOL 35C scanning electron microscope (SEM) with an accelerating voltage of 15 kV was used for fractographic studies.

3. ANALYTICAL MODEL

3.1 Stress Analysis

The basic assumptions for elastic stress analysis, proposed by Goland and Reissner[31] for joints, are used in this study. Edde and Verreman[14] have used a similar procedure to achieve a general stress solution for the cracked-lap shear (CLS) specimens. The CPS specimen (Fig. 1) is made up of two adherends of equal height, H, and width, b, respectively, bonded together along the bond line, L, with an adhesive thickness, t. Figure 2a illustrates the force equilibrium for an element with length dx in the adhesive joint. If the bond thickness, t, is much smaller than other dimensions of the specimen, it can be assumed that only shear stress is present at the interface between the adherends and the adhesive. Using the superposition principle, the equivalent forces and moments as well as corresponding strain distributions are shown in Figure 2b and c, respectively. Assuming both adherends bend with the same radius of curvature so that bending contributes to the shear stress in the adhesive but does not produce a peel stress, equilibrium in the x direction requires:

$$\begin{aligned} -F_1 - \tau dx + F_1 + \frac{\partial F_1}{\partial x} dx = 0 \\ -F_2 + \tau dx + F_2 + \frac{\partial F_2}{\partial x} dx = 0 \end{aligned} \tag{2a}$$

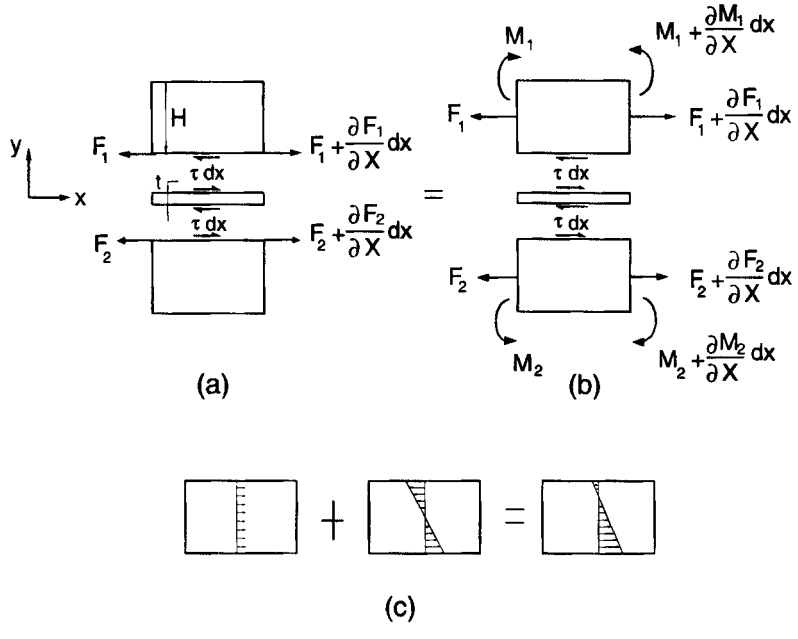

FIGURE 2 Force and displacement distributions of element dx using superposition principle.

i.e.

$$\frac{\partial F_1}{\partial x} = \tau$$
$$\frac{\partial F_2}{\partial x} = -\tau \tag{2b}$$

Since $M_1 = F_1 H/2$, $\partial M_1/\partial x = (\partial F_1/\partial x)(H/2)$, considering a plane strain condition for the adherends, the strains at the two interfaces of the adhesive and the adherends are given by:

$$\varepsilon_{x1} = \frac{du_1}{dx} = (1-\nu^2)\left(\frac{F_1}{E_{al}H} + 6\frac{M_1}{E_{al}H^2}\right) = \frac{4F_1(1-\nu^2)}{E_{al}H} \tag{3}$$

Similarly,

$$\varepsilon_{x2} = \frac{du_2}{dx} = \frac{4F_2(1-\nu^2)}{E_{al}H} \tag{4}$$

where E_{al} is the Young's modulus and ν the Poisson's ratio of the aluminium adherend. The expressions for the shear strain and shear stress within the adhesive layer are:

$$\gamma = \frac{u_1 - u_2}{t} \tag{5}$$

$$\tau = \gamma\mu = \frac{u_1 - u_2}{t}\mu \tag{6}$$

where γ is the shear strain, u_1 and u_2 the displacements in the x direction at the interface lines and μ the shear modulus of the adhesive. Using Equations (3), (4) and (6), the relation between the shear stress and the displacements is given by:

$$\frac{d\tau}{dx} = \frac{d(u_1 - u_2)}{dx}\frac{\mu}{t} = \frac{4\mu(1-\nu^2)(F_1 - F_2)}{E_{al}Ht} \tag{7}$$

$$\frac{d^2\tau}{dx^2} = \frac{4\mu(1-\nu^2)}{E_{al}Ht}\left(\frac{dF_1}{dx} - \frac{dF_2}{dx}\right) \tag{8}$$

Substituting Equation (2b) in (8) gives:

$$\frac{d^2\tau}{dx^2} - \frac{8\mu(1-\nu^2)}{E_{al}Ht}\tau = 0 \tag{9}$$

or

$$\frac{d^2\tau}{dx^2} - \beta^2\tau = 0 \tag{10}$$

where

$$\beta = \sqrt{\frac{8\mu(1-\nu^2)}{E_{al}Ht}} \tag{11}$$

The general solution of Equation (10) is:

$$\tau = C_1 e^{\beta x} + C_2 e^{-\beta x} \tag{12}$$

Assuming a semi-infinite CPS specimen with a sufficiently long joint, the following boundary conditions are applied:

$$\begin{aligned} &\tau(x=0)=0 \\ &\int_0^L \tau dx = P \end{aligned} \tag{13}$$

where P is the applied load per unit length. Thus, using Equations (12) and (13) gives:

$$\begin{aligned} C_2 &= -C_1 \\ C_1 &= \frac{P\beta}{2[\mathrm{Cosh}(\beta L)-1]} \end{aligned} \tag{14}$$

Then, the shear stress along the bond line is given by:

$$\tau = \frac{P\beta}{[\mathrm{Cosh}(\beta L)-1]}\mathrm{Sinh}(\beta x) \tag{15}$$

Figure 3 shows the distributions of the shear stress along the bond line in the joints of different bond thickness when $\mu = 1.16\,\mathrm{GPa}$, $\nu = 0.3$ and a load of (100 N/mm) is applied. The maximum shear stress, τ_{max}, occurs at the crack tip. As the bond thickness,

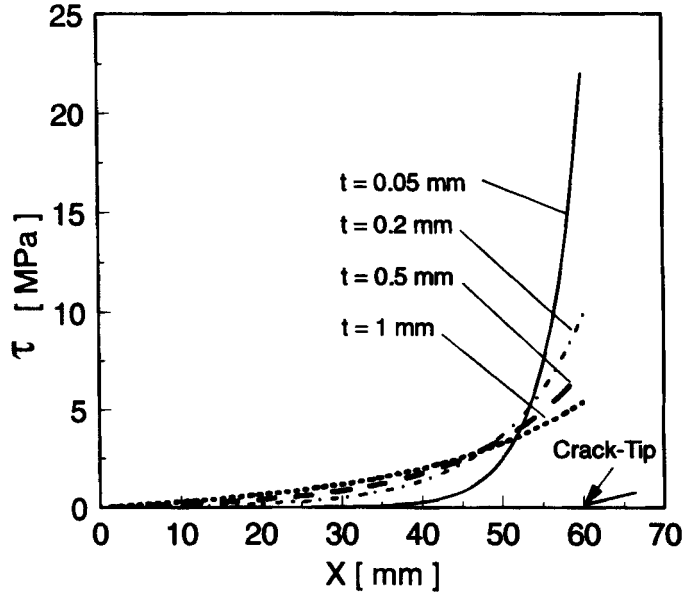

FIGURE 3 Distributions of shear stress along the adhesive bond line for different t.

t, is decreased, the value of τ_{max} increases significantly near the crack tip. When $t < 0.1$ mm, the major part of the bond line is unstressed and a sharp rise occurs at the crack tip, whereas when $t > 0.1$ mm, the shear stress is gradually enhanced over the whole bond line with a high gradient near the crack tip.

3.2 Mode-II Strain Energy Release Rate, G_{II}

The fracture of homogeneous materials can be described in term of two fracture parameters, *i.e.* stress intensity factor, K, and strain energy release rate, G. These two parameters have been widely used in the characterisation of mode-I and mode-II fractures of adhesive joints.[1-16,24-27] The stress intensity factor approach presumes a singular stress state at the crack tip, which presents some theoretical difficulties in the case of bimaterials. In the stress analysis of the previous section, the pure shear model does not consider the crack tip singularity. However, the analysis can be used directly to evaluate the mode-II strain energy release rate.

The crack closure method[32] associated with virtual crack extension is used to evaluate the mode-II strain energy release rate, G_{II}, of the adhesive joints assuming the crack propagates at the interface between the adherend and the adhesive (Fig. 4) *i.e.*:

$$G_{II} = \operatorname*{Lim}_{\Delta a \to 0} \frac{1}{2\Delta a} \int_{L-\Delta a}^{L} \tau(u_1 - u_2) dx \tag{16}$$

Substituting Equations (5) and (6) to (16) and integrating:

$$G_{II} = \frac{t}{2\mu} \frac{P^2 \beta^2 \mathrm{Sinh}^2(\beta L)}{[\mathrm{Cosh}(\beta L) - 1]^2} \tag{17}$$

where the adhesive bond thickness, t, is involved, which was, however, ignored in most previous analytical studies.[9,23]

4. FINITE ELEMENT APPROACH

To verify the analytical model developed in the previous section, a two-dimensional finite element model (FEM) shown in Figure 5 was generated to evaluate the stress distributions and the mode-II energy release rate of the CPS specimens. The shear loads were applied to the model far enough from the crack-tip to prevent any localised

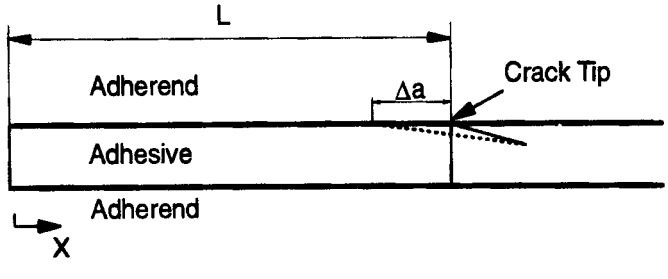

FIGURE 4 Interfacial crack extension at the crack tip.

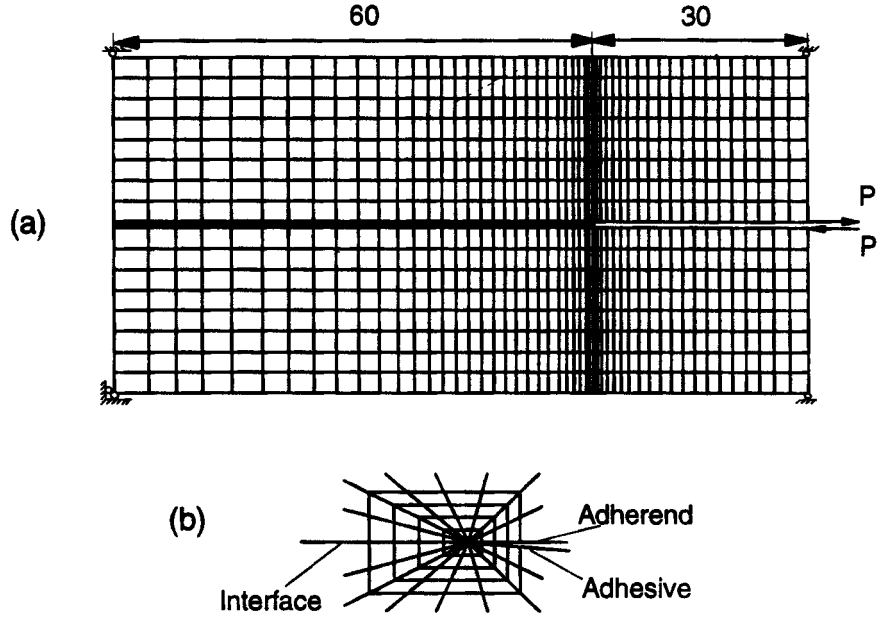

FIGURE 5 (a) A typical finite element model of CPS specimen, and (b) crack tip configuration.

effect on the crack-tip stress distribution. All finite element analyses (FEA) were conducted assuming linear-elastic behaviour for both adherends and adhesive. Eight-noded quadrilateral plane strain elements were used, and coarse meshes were applied for the adherends whilst fine meshes were used around the crack tip region for the adhesive. Singular elements were employed to evaluate the stress state around a sharp crack tip which is located at the interface between the adhesive and the adherend. Figure 5b illustrates the crack-tip elements configuration. Mode-II strain energy release rate was evaluated from the difference in strain energies of two different crack lengths;[32] one with crack length a and the other with crack length $a + \Delta a$, *i.e.*:

$$G_{II} = \frac{U(a + \Delta a) - U(a)}{\Delta a} = \frac{\Delta U}{\Delta a} \tag{18}$$

All analyses were carried out by the ADINA[33] software. The shear stress distribution from FEA agrees well with the analytical results (Eq. 15) when $t = 0.2$ mm, as shown in Figure 6. It can be seen that the shear stress near the crack-tip increases sharply due to the singularity in FEA. Similar behaviour was obtained for other bond thickness.

5. RESULTS AND DISCUSSION

5.1 Fracture Mechanisms

Figure 7 shows the fracture loads, P_C, obtained from experiments for a constant crack length when the adhesive bond thickness was varied from 0.02 mm to 0.9 mm. The

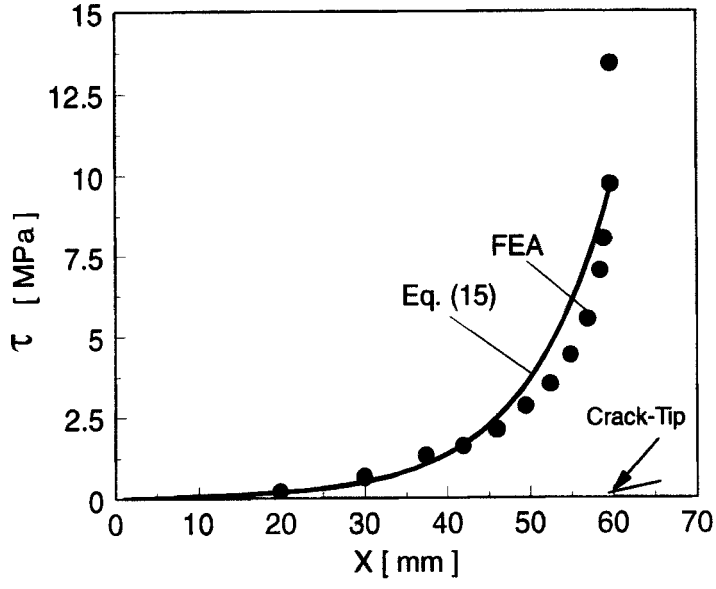

FIGURE 6 Comparison of shear stress distribution along the adhesive bond line for $t = 0.2$ mm by FEA and Equation (15).

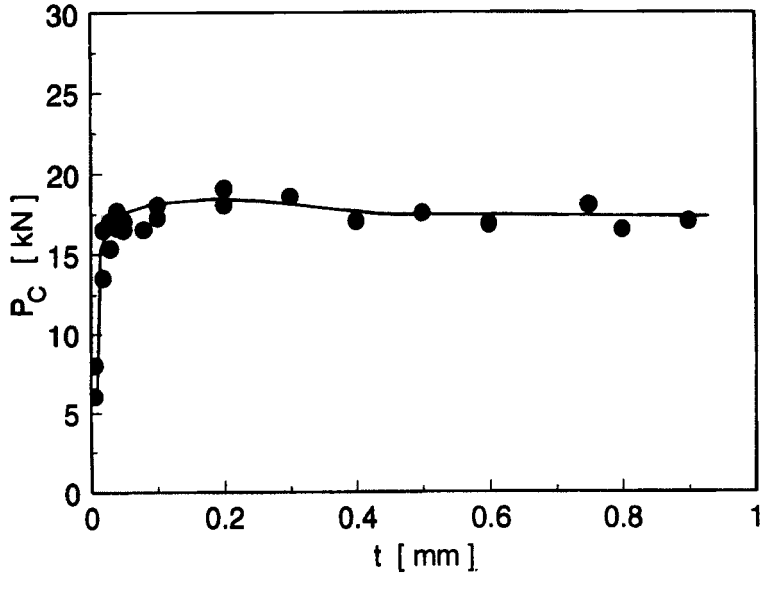

FIGURE 7 Variation of fracture load, P_C, *versus* bond thickness, t.

fracture load rises very sharply when $t < 0.03$ mm, whilst a gradual increase in P_C is observed when $0.03\text{ mm} < t < 0.1$ mm. For $0.1 < t < 1$ mm, P_C is almost independent of the bond thickness. This can be attributed to the interfacial debonding of the CPS adhesive joints where the crack propagated mostly along the interface between the adherend and the adhesive. SEM fracture morphology of the CPS adhesive joints shows that, when $t < 0.1$ mm, the crack initiated from the pre-crack tip immediately deflected and propagated afterwards along the interface. In particular, for the adhesive joints with very small bond thickness ($t < 0.03$ mm), the path of crack propagation in some regions periodically jumped between the two interfaces. Therefore, a typical pattern of a fracture surface was the isolated adhesive islands distributed on the adherend surface (Fig. 8). When $t > 0.1$ mm, two different crack paths were observed. In most specimens, despite using a release agent between the Teflon film and the spacer in specimen preparation (Fig. 1), the crack initiated from the location where the spacer was attached to the adherend, then the crack propagated along the interface between the adherend and the adhesive. However, for a few specimens with large bond thickness ($0.7\text{ mm} < t < 0.9$ mm), the crack initiated from the pre-crack tip and proceeded at a particular angle towards the adherend, then propagated along the interface. This was attributed to the non-coplanar crack extension in resins under pure sliding as proposed by some investigators.[34–36] A physical model for this mechanism following References 35 and 36 is shown in Figure 9a. It is postulated that under pure sliding the crack propagates in the direction perpendicular to the maximum normal stress. The angle of crack propagation, θ, for a specimen with $t = 0.8$ mm was measured using a special technique. A soft hydrophilic polysiloxane polymer (GC, Co., Japan) was first used to replicate the crack-front region of the post fracture surface. Then parallel slices were cut

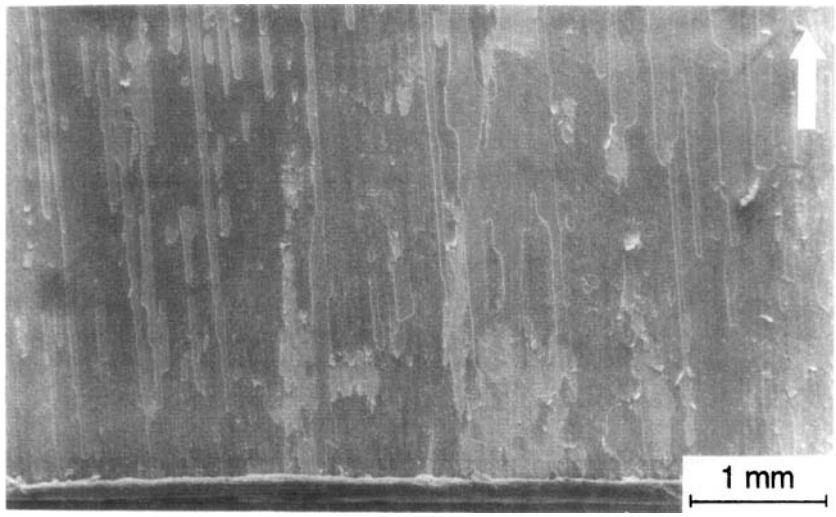

FIGURE 8 Fracture surface morphology of an adhesive joint with $t = 0.02$ mm. (Arrow indicates direction of crack propagation).

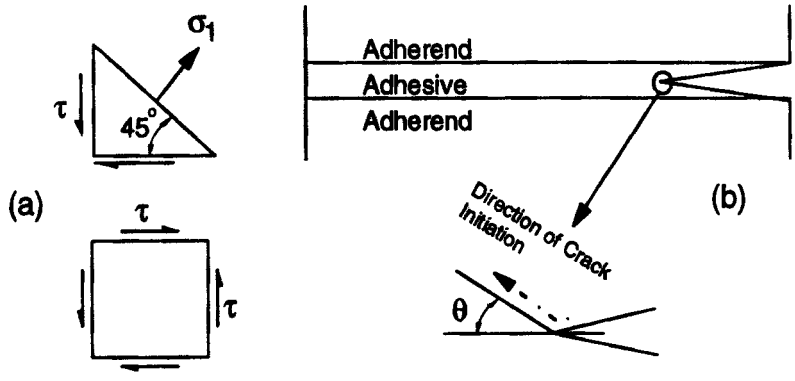

FIGURE 9 Physical model explaining direction of crack growth under mode-II sliding.

from the crack-front region and the angle of crack initiation was measured using a Nikon profile projector. The observed angle varied from 33° to 40° along the crack front, which is consistent with the model illustrated in Figure 9b. The prediction with the maximum normal stress criterion[35,36] indicates that the crack propagates with an angle of 45° under the pure sliding mode.

The post-fracture surface of specimens with different bond thickness shows a similar morphology. Further inspection of the fracture surface using SEM at high magnification reveals that areas of scallops result from the last crack propagation (Fig. 10). However, different interfacial fracture paths with varying degree of plastic deformation were observed when the crack proceeded from the adhesive towards the adherend (Fig. 11). This mechanism was found to be clearly dependent on the bond thickness, and could be correlated with the constraint effect of the adherends, which suppressed and prevented the plastic deformation for small bond thickness.[13]

5.2 Fracture Energy

Figure 12 shows the mode-II strain energy release rate, G_{II}, of the CPS specimens for an applied load of 100 N/mm. The results calculated from Equation (17) indicate that G_{II} remains almost a constant for bond thickness less than 0.2 mm and, thereafter, a gradual increase with bond thickness is obtained. The numerical FEA results show a linear increase of G_{II}, with bond thickness similar to the theoretical curve. This indicates that, as the constraint of the adherends is reduced, the stress state at the crack tip is relieved (see Fig. 3) allowing more plastic deformation of the adhesive to take place. Hence, the adhesive material can absorb more energy before fracture. For comparison, the G_{II} values obtained from Equation (1), proposed by Ripling *et al.*[23] is also shown in Figure 12. In Equation (1), it is assumed that the applied force produces a uniform deformation along the height of the adherends. This assumption is acceptable when the ratio of the length to the height of the adherend (L/H) is quite large, which is normally the case in the lap-shear joints. However, because the applied shear force on the CPS specimens causes only a local deformation around the crack tip, a non-uniform strain

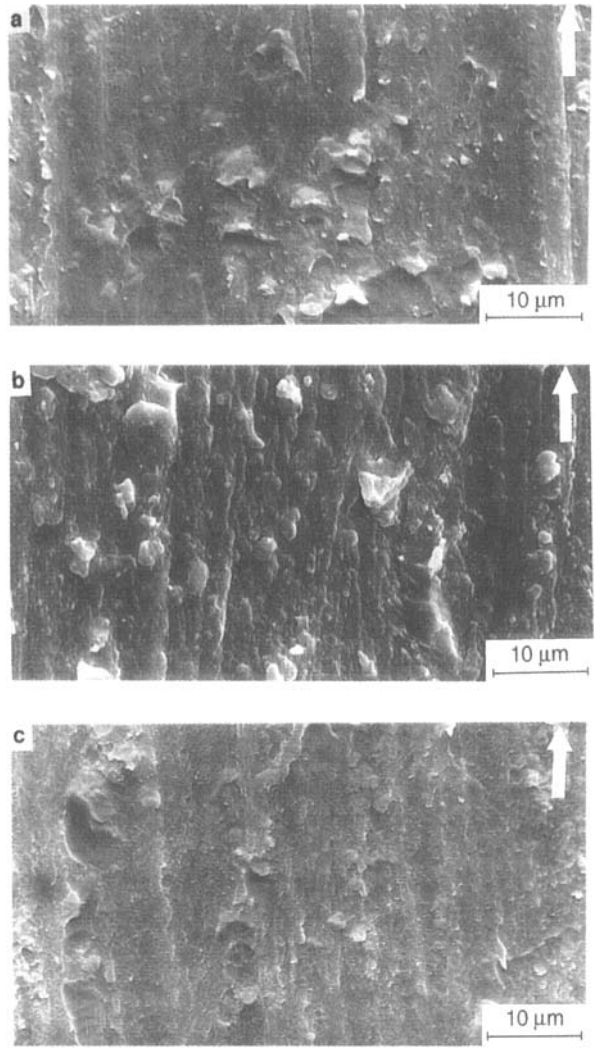

FIGURE 10 Fracture surface morphology of adhesive joints with (a) $t = 0.02$ mm, (b) $t = 0.1$ mm, and (c) $t = 0.6$ mm. (Arrow indicates direction of crack propagation).

distribution in the adherend seems more reasonable. Therefore, a considerable difference in G_{II} values evaluated by Equation (1) and those from the present study is observed in Figure 12.

The mode-II critical strain energy release rate (i.e. fracture energy), G_{IIC}, was evaluated from Equation (17) using the fracture load, P_C. The variation of G_{IIC} and mode-I fracture energy, J_{IC}, as a function of the adhesive bond thickness, is shown in Figure 13. The data for J_{IC} were obtained in the previous studies[12] from the CT adhesive joints using the J-integral method in the FEA. As shown in Figure 13, a sharp

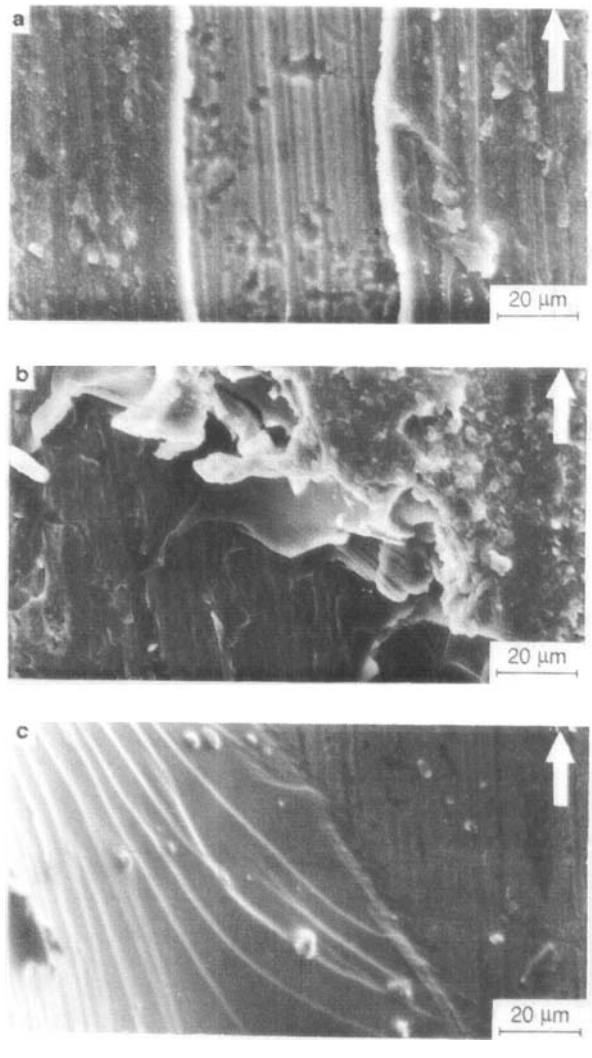

FIGURE 11 Fracture surface morphology at the interface of adherend and adhesive in adhesive joints with (a) $t = 0.02$ mm, (b) $t = 0.03$ mm, and (c) $t = 0.8$ mm. Plastic deformation at interface is observed in (b) and (c). (Arrow indicates direction of crack propagation).

rise of G_{IIC} is obtained for very small bond thickness ($t < 0.03$ mm), while a gradual increase occurs for $t > 0.03$ mm. This trend is similar to that obtained for a BP-907 modified epoxy.[15] When the adhesive thickness is very small ($t < 0.03$ mm), the constraint of the adherends severely limits the deformation of the adhesive material and brittle fracture results. However, as the constraint of the adherends is reduced, due to the shear deformation at the crack tip, the adhesive material can absorb more energy before fracture. Comparison between G_{IIC} and J_{IC} indicates that for different bond thickness, the joint is at least an order of magnitude tougher in shear than in tension.

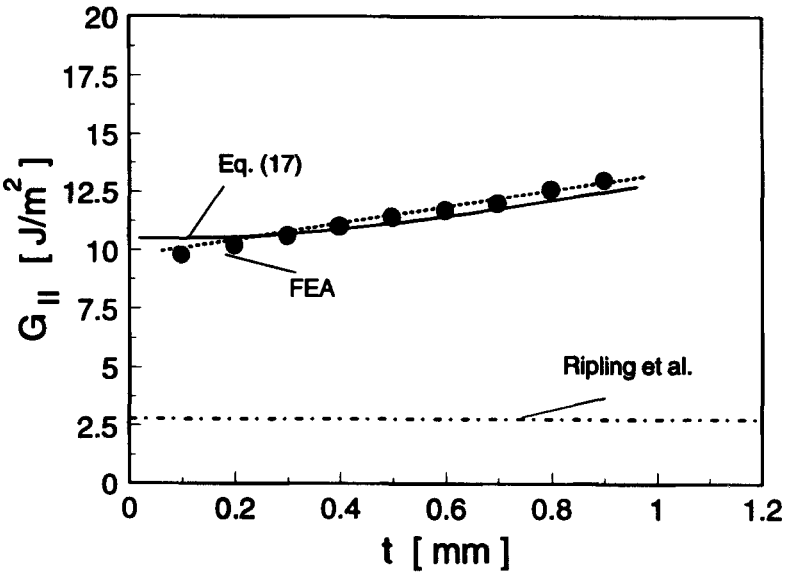

FIGURE 12 Variation of mode-II strain energy release rate, G_{II}, as a function of bond thickness, t. (Applied load P is 100 N/mm).

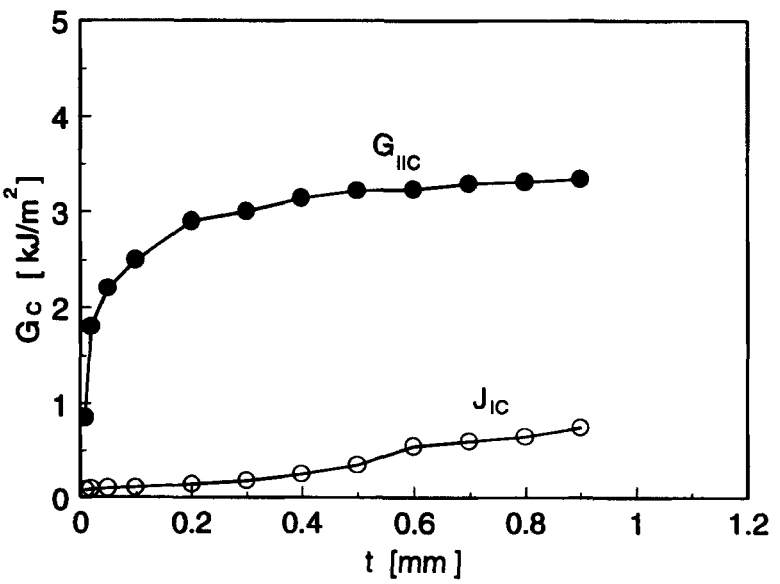

FIGURE 13 Variation of G_{IIC} and $J_{IC}^{1,2}$ as a function of bond thickness, t.

These results are consistent with the results obtained by Chai[15] and Ripling *et al.*[23] For the rubber-modified epoxies, mechanisms such as crazing and void formation followed by shear bands can contribute to increase the fracture energy. In the absence of these mechanisms,[28] particularly when the material is suppressed between the adherends, a

low value of J_{IC} is normally expected. On the other hand, under the sliding mode-II fracture, shear deformation is the main mechanism to dissipate the energy and, therefore, a much higher mode-II toughness than mode-I toughness is obtained because of very high shear stress in the bond line.[37]

5. CONCLUSIONS

Compact pure shear specimens (CPS) were used to study the mode-II sliding fracture behaviour of aluminium-epoxy adhesive joints with different bond thickness. It was found that, at the present applied strain rate, the fracture load depended on the bond thickness, t, which increased very rapidly for very small bond thickness ($t < 0.03$ mm), followed by a more gradual increase when 0.03 mm $< t <$ 0.1 mm, and remained almost constant for larger bond thickness (0.1 mm $< t <$ 1 mm). SEM studies on the fracture surfaces of specimens with different bond thickness showed a mainly interfacial failure path with a brittle fracture appearance. An analytical model based on elastic stress analysis was developed to evaluate stress distributions along the adhesive bond line. The results indicated that for small bond thickness ($t < 0.1$ mm), the major part of the bond line remained unstressed, but the shear stress rose sharply near the crack tip. For $t > 0.1$ mm, a gradual increase of the shear stress occurred along the whole bond line. The crack-closure technique was applied to evaluate the mode-II strain energy release rate, G_{II}, of the adhesive joints using the results of the stress analysis. A finite element model (FEM) was also developed to evaluate the stress state along the bond line and the energy release rate of the CPS specimens. The results of the finite element analyses (FEA) were consistent with the analytical studies. For a given applied load, G_{II} gradually increased as the bond thickness is increased. The critical strain energy release rate, G_{IIC}, was determined using the fracture load of specimens. It was found that G_{IIC} rose sharply for very small bond thickness ($t < 0.03$ mm), and then increased gradually for larger bond thickness ($t > 0.03$ mm). These results could be explained in terms of the reduction of crack tip constraint as the bond thickness increased.

Acknowledgements

The authors wish to thank the Electron Microscope Unit at the University of Sydney for access to its facilities. H. R. Daghyani was supported by a scholarship from the Ministry of Culture and Higher Education of Iran (MCHE).

References

1. G. P. Anderson and K. L. DeVries, in *Treatise on Adhesion and Adhesives*, Vol. 6, R. L. Patrick, Ed. (Marcel Dekker, Inc., New York, 1989).
2. H. Chai, *Engng. Fract. Mech.*, **20**, 413 (1986).
3. S. Mall and G. Ramamurthy, *Int. J. Adhesion Adhesives*, **9**, 33 (1989).
4. S. S. Wang, J. F. Mandell and F. J. McGarry, *Int. J. Fract.*, **14**, 39 (1978).
5. G. P. Anderson, S. J. Bennett and K. L. DeVries (Academic Press, New York, 1977).
6. J. H. Crews, Jr., K. N. Shivakumar and I. S. Raju, *Adhesive Bonded Joints: Testing and Design*, **ASTM STP 981**, W. S. Johnson, Ed. (American Society for Testing and Materials, Philadelphia, 1988), pp. 119–132.

7. J. M. Scott and D. C. Phillips, *J. Mater. Sci.*, **10**, 551 (1975).
8. G. G. Trantina, *J. Comp. Mater.*, **6**, 192 (1972).
9. Y.-W. Mai and A. S. Vipond, *J. Mater. Sci. Letts.*, **13**, 2280 (1978).
10. S. F. Stone, R. A. Westman and M. F. Fourney, "Analytical and Experimental studies in Adhesive Mechanics", *UCLA-ENG-7556*, July 1975.
11. S. A. Hamoush and S. H. Ahmad, *Int. J. Adhesion Adhesives*, **35**, 171 (1989).
12. H. R. Daghyani, L. Ye and Y.-W. Mai, *J. Adhesion*, **53**, 149 (1995).
13. H. R. Daghyani, L. Ye and Y.-W. Mai, *J. Adhesion*, **53**, 163 (1995).
14. F. Edde and Y. Verreman, *Int. J. Adhesion Adhesives*, **12**, 43 (1992).
15. H. Chai, *Int. J. Fract.*, **37**, 137 (1988).
16. H. Chai, *J. Mater. Sci.*, **28**, 4944 (1993).
17. G. Fernuld and J. K. Spelt, *Int. J. Adhesion Adhesives*, **11**, 213 (1991).
18. G. Fernuld and J. K. Spelt, *ibid.* **11**, 221 (1991).
19. S. S. Wang, J. F. Yau, *Int. J. Fract.*, **19**, 295 (1982).
20. F. Delale, F. Erdogan and M. Ydinoglu, *J. Comp. Mater.*, **15**, 249 (1985).
21. M. Ratwani and H. Kan, *Comp. Sci. & Tech.*, **23**, 53 (1985).
22. A. J. Russell, Proc. ASME Symposium on "Advances in Adhesively Bonded Joints", Chicago, IL, U.S.A., Nov. 28–Dec. 2, 1988, pp. 87–92.
23. E. J. Ripling, S. Mostovoy and R. L. Patrick, in **ASTM STP 360**, (American Society for Testing and Materials, Philadelphia, 1963), p. 5.
24. S. N. Chatterjee, V. Ramnath, W. A. Dick and Y. Z. Chen, *Composite Materials: Testing and Design (Ninth Volume)*, **ASTM STP 1095**, S. P. Garbo, Ed. (American Society for Testing and Materials, Philadelphia, 1990), pp. 324–346.
25. G. K. Hu and D. Francois, *J. Adhesion*, **37**, 261 (1992).
26. F. Farhad, R. Muki and R. A. Westman, *Int. J. Solids Structures*, **13**, 561 (1977).
27. S. S. Wang, Fracture Mechanics, **ASTM STP 677**, C. W. Smith, Ed. (Am. Society for Testing and Materials, Philadelphia, 1979), pp. 651–667.
28. H. R. Daghyani, L. Ye, Y.-W. Mai and J. S. Wu, *J. Mater. Sci. Letts*, **13**, 1330 (1994).
29. I.-M. Low and Y.-W. Mai, *Comp. Sci. Tech.*, **33**, 191 (1988).
30. A. F. Yee and R. A. Pearson, *J. Mater. Sci.*, **21**, 2462 (1986).
31. M. Goland and E. Reissner, *J. Appl. Mech.*, **11**, A17 (1944).
32. E. F. Rybicki and M. F. Kanninen, *Engng. Fract. Mech.*, **9**, 931 (1977).
33. ADINA R & D, Inc., USA, 1992.
34. J. G. Williams, "*On Fracture Mechanics of Polymers*" (Ellis Horwood Limited, England, 1984), pp. 74–78.
35. L. Arcan, M. Arcan and I. M. Daniel, *Fractography of Modern Engineering Materials: Composites and Metals*, **ASTM STP 984**, J. E. Masters and J. J. Au, Eds. (American Society for Testing and Materials, Philadelphia, 1987), pp. 41–67.
36. B. W. Smith and R. A. Grove, *Fractography of Modern Engineering Materials: Composites and Metals*, **ASTM STP 984**, J. E. Masters and J. J. Au, Eds. (American Society for Testing and Materials, Philadelphia, 1987), pp. 154–153.
37. W. S. Johnson and P. D. Mangalgir, *Toughened Composites*, **ASTM STP 937**, N. J. Johnson, Ed. (American Society for Testing and Materials, Philadelphia, 1987), pp. 295–315.